Moving Contact Lines of a Colloidal Suspension in the Presence of Drying

E. Rio,*,† A. Daerr,†,‡ F. Lequeux,§ and L. Limat†,‡

Laboratoire de Physique et Mécanique des Milieux Hétérogènes, 10 rue Vauquelin, 75 005 Paris France, UMR CNRS 7636, Laboratoire Matière et Systèmes Complexes, UMR CNRS 7057, and Laboratoire de Physico-Chimie des Polymères et des Milieux Dispersés, 10 rue Vauquelin, 75 005 Paris France, UMR CNRS 7615

Received November 7, 2005. In Final Form: February 2, 2006

This article presents the first experimental study of an advancing contact line for a colloidal suspension. A competition between the hydrodynamic flow due to the drop velocity and the drying is exhibited: drying accounts for particle agglomeration that pins the contact line whereas the liquid flow dilutes the agglomerated particles and allows the contact line to advance continuously. The dilution dominates at low concentration and high velocity, but at high concentration and low velocity, the contact line can be pinned by the particle agglomeration, which leads to a stick−slip motion of the contact line. The calculation of the critical speed splitting both regimes gives an order of magnitude comparable to that of experiments. Moreover, a model of agglomeration gives an estimation of both the size of the wrinkles formed during stick−slip and the force exerted by the wrinkle on the contact line.

1. Introduction

Coating a solid surface with colloid layers of uniform thickness is a challenge of central importance in many industrial applications. A typical example is the control of optical properties of glasses that can be tuned at will with appropriate colloidal compounds.[1,2]

Perhaps the simplest method consists of using flow-coating or spin-coating techniques:[3,4] in these processes, a contact line moves on the substrate such that the suspension invades the entire surface. Then, the obtained film dries and is supposed to leave a regular arrangement of colloids on the surface. However, as we shall see here, the situation is more complicated because the drying in fact begins as soon as the contact line advances. Because the evaporation rate is singular at the contact line,[5] coupling between the contact line motion and colloid deposition occurs that can lead to stick−slip oscillations of the contact line with heterogeneities of the final colloid layer. To our knowledge, this phenomenon, despite its central importance, has never been reported for an advancing contact line. We present here both the evidence of its occurrence on an advancing contact line and a quantitative study of its influence on the contact line motion and colloid deposition.

Until now, the drying of colloidal suspensions has widely been studied in terms of 2D colloidal crystal formation.[6−8] In another direction, the drying of sessile drops deposited on a solid has also received great attention.[5,9−11] Deegan et al. showed by analogy with electrostatics that the evaporation rate is singular at the contact line: if one considers the drop and its reflection in the substrate, then a tip effect concentrates the evaporation lines near the contact line, which makes the evaporation rate diverge. This one reads $J_0 x^{-\alpha}$, where x is the distance to the contact line and α is an exponent that depends on the contact angle ($\alpha = 1/2$ at low contact angle). Consequently, the evaporation losses of the solvent account for the motion of the solute species toward the contact line. This motion results in the concentration of the particles and thus in flocculation. Hence, the solute species tend to accumulate around the contact line, pinning the line on the substrate. Particle agglomeration is at the origin of the ringlike deposit commonly observed around drying coffee drops. Under certain conditions, this deposition can also lead to multi-ring deposits when the contact line is alternatively pinned or unpinned during evaporation.[12,13] Similar multideposits have also been observed in capillary tubes with latex suspensions.[14]

In all of these recent works pertaining to drop evaporation, one is faced with a static contact line or at least with a receding contact line at very low velocity (quasistatic situation), but no work deals with an advancing contact line, possibly at high velocity as occurs in many industrial applications. To study this novel situation, we performed experiments in which a drop of a colloidal suspension is pushed on a solid surface. A stick−slip motion of the contact line can be observed for special values of the suspension concentration and of the drop velocity. A dynamic phase diagram recording these values is proposed in this article. Then some SEM (scanning electronic microscope) pictures show the deposit due to the stick−slip motion. In this article, we propose two models to describe the peculiar behavior of the droplets. In the first, we discuss the competition between flows induced

† Laboratoire de Physique et Mécanique des Milieux Hétérogènes, UMR CNRS 7636.

‡ Laboratoire Matière et Systèmes Complexes, UMR CNRS 7057.

§ Laboratoire de Physico-Chimie des Polymères et des Milieux Dispersés, UMR CNRS 7615.

(1) Belleville, P. *Verre* **2000**, 206.
(2) Maenosono, S.; Dushkin, C. D.; Saita, S.; Yamaguchi, Y. *Langmuir* **1999**, *15*, 957.
(3) Mennig, M.; Schmidt, H. http://www.solgel.com/articles/Nov00/mennig.htm.
(4) Kistler, S. F.; Schweizer, P. M. *Liquid Film Coating*; Chapman & Hall: New York, 1997.
(5) Deegan, R. D.; Bakajin, O.; Dupont, T. F.; Huber, G.; Nagel, S. R.; Witten, T. A. *Nature* **1997**, *389*, 827.
(6) Denkov, N. D.; Velev, O. D.; Kralchevsky, P. A.; Ivanov, I. B.; Yoshimura, H.; Nagayama, K. *Langmuir* **1992**, *8*, 3183.
(7) Dimitrov, A. S.; Nagayama, K. *Langmuir* **1996**, *12*, 1303.
(8) Pieranski, P.; Strzelecki, L.; Pansu, B. *Phys. Rev. Lett.* **1983**, *12*, 900.
(9) Deegan, R. D.; Bakajin, O.; Dupont, T. F.; Huber, G.; Nagel, S. R.; Witten, T. A. *Phys. Rev. E* **1999**, *62*, 756.
(10) Parisse, F.; Allain, C. *Langmuir* **1997**, *13*, 3598.
(11) Gorang, Y.; Pauchard, L.; Calligari, G.; Hulin, J.-P.; Allain, C. *Langmuir* **2004**, *20*, 5138.
(12) Shmuylovitch, L.; Shen, A. Q.; Stone, H. A. *Langmuir* **2002**, *18*, 3441.
(13) Adachi, E.; Dimitrov, A. S.; Nagayama, K. *Langmuir* **1995**, *11*, 1057.
(14) Abkarian, M.; Nunes, J.; Stone, H. A. *J. Am. Chem. Soc.* **2004**, *126*, 5978.

10.1021/la052989e CCC: $33.50
Published on Web 03/03/2006

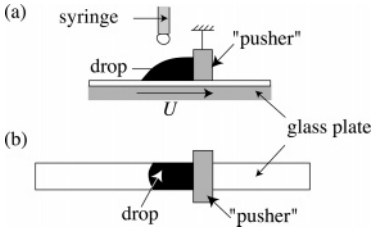

Figure 1. Scheme of the setup used to push a drop: (a) side view and (b) top view. A glass plate is advancing at speed U under the droplet. To avoid the droplet motion, a fixed Teflon pusher keeps the drop from advancing.

respectively by evaporation and contact line motion, which accounts for the critical velocity. Beyond this velocity, the contact line can pin onto the substrate, and a stick−slip motion is observed. The second model allows us to describe the contact line behavior during the stick−slip motion. In particular, the amplitude of the stick−slip is calculated and compared to the experiments.

2. Experiments

2.1. Pushed Droplets. We performed the experiments on a suspension of silica particles (monodisperse, 90 nm diameter) synthesized using the Stober method.[15] The particles were washed in distilled water by dialysis, the pH was adjusted to 9, and the ionic strength was adjusted up to 10^{-2} M using KNO_3. The available suspension has a concentration of $\phi = 400$ g/L (i.e., a volumic fraction of $\Phi \simeq 18\%$) and a relative density of $d = 2.25$. It was diluted with distilled water, and the pH was adjusted to 9 after each dilution. We thus obtained suspensions of concentrations $\phi = 20$, 40, 100, 200, and 300 g/L ($\Phi = 0.9$, 1.8, 4, 9, 13% by volume).

The glass cleaning is a critical and delicate phase of the experiment. Using a perfectly wetable substrate for water, such as freshly cleaved mica, leads to a spontaneous advance of the contact line of a water droplet. Because we want to control the velocity of the contact line, we have to choose a surface that is not spontaneously wetted by water. However, some wettability defects can indeed pin the contact line even with a drop of pure water and have to be avoided. Moreover, we have to use a surface that gives reproducible results. We finally choose the following protocol that has been found to give reproducible results. The following process is then carefully and systematically applied: first, the glass is slightly polished with cerium oxide particles (CeroxGG, provided by Rhodia) of about 2 μm diameter, which have been diluted in distilled water to up to 20% by mass. Then it is rinsed successively with tap water, ethanol, and distilled water. Finally, the plate is dried by clean compressed air and dried in a flame. On the obtained substrate, a sessile water droplet exhibits a very low contact angle on the order of 10°.

Figure 1 shows the experimental setup. A syringe allows us to deposit a drop of controlled volume (50 μL) on a clean glass plate of large aspect ratio (15 × 0.8 cm). The glass plate is fixed on a translating table linked to a motor that controls the translation velocity U (on the order of 1 to 10 mm/s in our experiment). The substrate moves with respect to the drop because a Teflon cube, called a "pusher" in picture 1, holds it back. A video camera records side views of the drop evolution during the glass translation. If a drop of pure water is put on the glass plate, then its shape is stationary: the drop is advancing at constant velocity with respect to the glass plate. Then, the contact angle does not depend significantly on the imposed velocity and is still around 10° ≃ 0.17 rad (dashed lines in Figure 3a). The whole experimental setup is contained in a box where the relative humidity is 40%. A fan is placed about 10 cm from the pusher, with an air flow of 10 m/s at the level of the droplet. The use of a fan is crucial because natural air convection is always present and thus the evaporation rate is uncontrolled in the absence of controlled air flux. The evaporation rate of water is then rather small and allows us to conduct the experiment without a significant change in the droplet volume over several minutes. However, because this evaporation rate is singular on the contact line it will prove to be sufficient to trigger the following phenomena. Unfortunately, it was not as easy to modify the humidity significatively in the box, but we have checked on other geometries, including swelling an axysymmetric droplet with a syringe, and have found that the humidity is indeed controlling the stick−slip phenomenon.

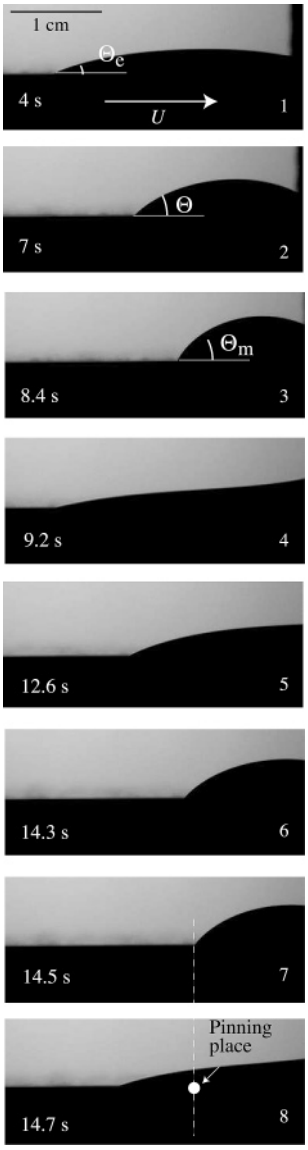

Figure 2. Stick−slip motion of the contact line of a droplet of concentration $\Phi = 18\%$ advancing at a speed $U = 0.8$ mm/s at successive times in seconds. We are in the droplet's frame, so if the contact line sticks on the glass plate, it goes in the right direction at speed U, and if it slips in a stationnary regime, it is static in this frame or moves sligthly to the right.

The experiment is now performed on a drop of a colloidal suspension. At low velocity and/or high concentration, a stick−slip motion of the contact line appears. Figure 2 shows this peculiar motion. Note that in the camera frame the substrate is moving from left to right at a speed U. Therefore, when the contact line is stuck to the glass plate (Figure 2, pictures 1−3 and 4−7), it follows the substrate motion and goes in the right direction. When the contact line slips on the substrate, the drop profile remains stationary in the laboratory frame. The periodic pinning accounts for large variations in the contact angle Θ during the experiment. We therefore measured $\Theta(t)$ (notation in Figure 2) on droplets of different concentrations advancing at different velocities. It varies between a minimum Θ_e and a maximum Θ_m.

(15) Stober, W.; Fink, A.; Bohn, E. *J. Colloid Interface Sci.* **1968**, *26*, 62.

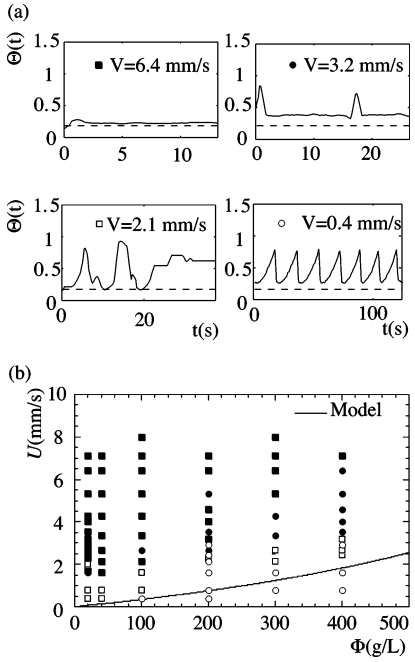

Figure 3. (a) Evolution of the contact angle Θ with the time *t*. Different regimes are observed on a suspension of concentration Φ depending on speed *U*. ■, Θ(*t*) constant. ●, Appearance of localized defects. □, Larger perturbations of the contact angle Θ. ○, Periodic stick−slip motion of the contact line and regular oscillation of the contact angle. (b) Phase diagram of the different regimes. The black line is obtained by the calculation presented in section 3.

Figure 3a shows the different functions Θ(*t*) observed at a given concentration Φ = 9% for different values of the velocity. First, at high velocity, here *U* = 6.4 mm/s, the drop shape is stationary as for a drop of pure water. The contact angle is therefore constant during the plate translation. Note that it is almost equal to the contact angle observed for pure water (dashed line). Then, for a smaller velocity of *U* = 3.2 mm/s, some infrequent jumps of the contact angle are observed. There is an amplification of these intermittent jumps defects at smaller velocity, here *U* = 2.1 mm/s, which corresponds to an intermittent motion of the contact line called stick−slip. Finally, when the plate advances very slowly, here *U* = 0.4 mm/s, the observed stick−slip motion becomes periodic. This peculiar motion is shown in Figure 2: the contact angle increases slowly during the pinning phase, falls suddenly as soon as the contact line slips, and increases again periodically.

These four regimes allow us to classify the different behaviors. The results are represented by the following symbols in Figure 3b: ■ if the drop shape is stationary, ● if some occasional defects appear, □ for irregular stick−slip, and ○ if periodic stick−slip is observed. The control parameters are the concentration Φ, which varies between 9 and 18, and the velocity *U*, which varies by 1 order of magnitude between 0.5 and 9 mm/s.

The phase diagram (Figure 3) shows that stick−slip (white symbols) appears at small velocity and high concentration, which suggests a competition between the drop velocity and the particle deposition. Moreover, some data, not shown here, have exhibited a strong effect of relative atmospheric humidity, which proves the importance of evaporation and drying in the process. This idea of a competition between deposition due to drying and drop velocity is the basis of the model proposed in the following text to describe this diagram.

2.2. SEM Visualizations. It is not possible to observe the particle deposition during the experiment using our setup. We therefore visualize the deposition after the experiment. A droplet of concentration Φ = 9 is pushed at a velocity of 0.4 mm/s on a clean glass plate. A stick−slip motion is observed under these conditions. The glass translation is stopped just after a slipping motion between the Teflon cube and the contact line, and a defect due to the pinning is expected (image 8 in Figure 2). The substrate is then turned upside down to remove most of the liquid. Unfortunately, some liquid remains on the substrate and dries before the visualization. The observed deposition is therefore partially due to this last drying phase. However, rinsing always leads to the destruction of the coating pattern, so we limited ourselves to this technique.

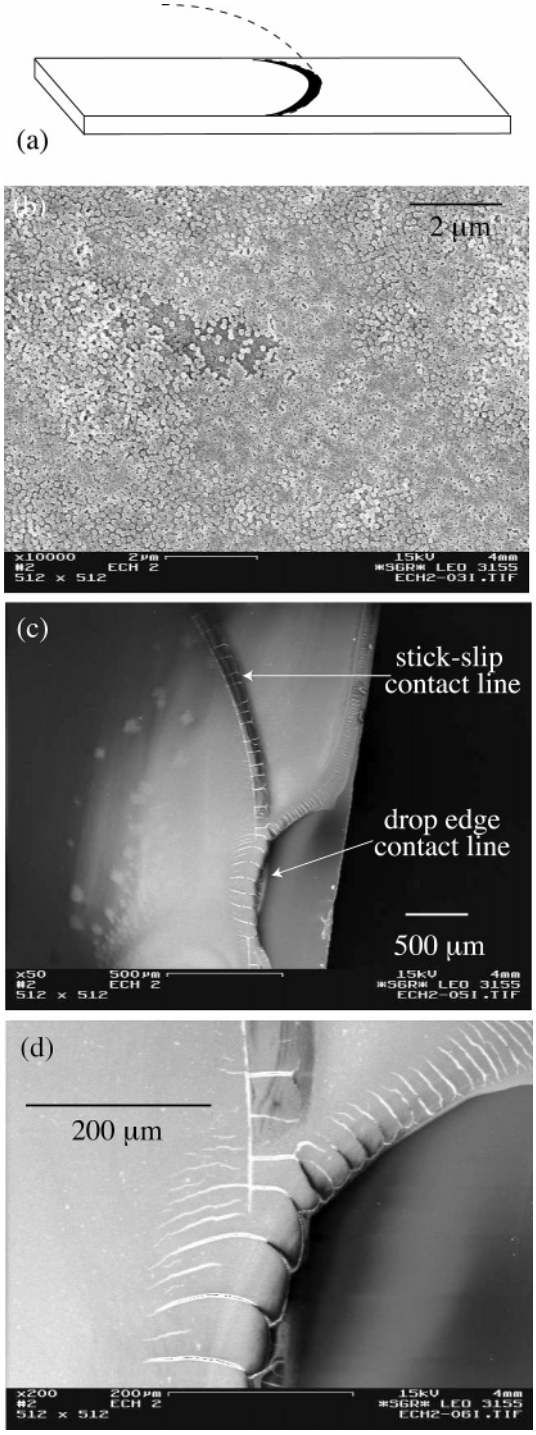

Figure 4. (a) Deposit left on the substrate is observed with a scanning elecronic microscope. Dashed line, former position of the drop. Black part, position of the wrinkle of particles left at the contact line. (b) Deposit out of the wrinkle (×10 000). (c) Deposit due to the stick−slip motion: observation of the particle wrinkle where the contact line has been stuck (×50). (d) Enlarged image of the particle wrinkle (×200).

The observation of the deposition gives a lot of information (Figure 4). In particular, a particle wrinkle appears where the contact line has been pinned (Figure 4b and c). Elsewhere, one or more layers of particles coat the glass plate almost homogeneously (Figure 4a).

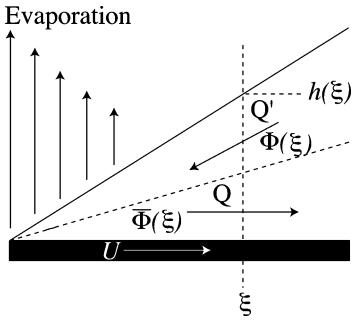

Figure 5. Notation used to calculate the competition between the concentration of the particles at the contact line due to evaporation and dilution due to the flow.

The wrinkle is very visible as soon as a contact line has been pinned because of the stick−slip at the drop edge (Figure 4b and c). These visualizations reinforce the idea that the pinning is linked to particle agglomeration at the contact line due to drying. This observation will lead to a first approach to calculate the size of this wrinkle in the second part of the following section.

3. Models

Two models are proposed in this section to explain the observed phenomena. First, two mechanisms are in competition: the contact line motion and the evaporation. The comparison of both of them leads to a critical speed above which the contact line can be pinned. This pinning threshold is plotted as a solid line in Figure 3b. Second, the amplitude (excursion of $\Theta(t)$) of the periodic stick−slip is calculated above the critical velocity. The comparison of the obtained amplitude with our data allows us to estimate the force exerted by the defect on the contact line.

3.1. Stationary Regime. We first consider a stationary contact line sliding freely on the solid, and we seek its pinning condition on the solid. The competition between liquid flow and evaporation can then be understood in terms of different fluxes for solvent and solutes. The evaporation tends to concentrate the particles in the vicinity of the contact line whereas liquid flow tends to make the concentration uniform, renewing the solution at the contact line. Let us write the water flux balance in a liquid wedge of length ξ at the contact line (Figure 5). This approximation of the free surface is very rough but allows us to capture most of the physics. It has often been used in the past to calculate simple approximations of the flow field involved in wetting dynamics with pure fluids.[16,17] In the stationary regime, the water flux entering this wedge, with the notations of Figure 5, reads $(1 - \Phi(\xi))Q'$, where Q' is the mean flow rate in the upper part of the wedge and $\Phi(\xi)$ is the mean particle concentration at a distance greater than ξ from the contact line. At the same time, the solid glass plate recedes and accounts for the liquid flow coming out of the wedge, which reads $(1 - \overline{\Phi(\xi)})Q$, where Q is the mean flow rate in the lower part of the drop and $\bar{\Phi}(\xi)$ is the mean concentration at a distance smaller than ξ from the contact line. Water also evaporates from the wedge with a flux, expressed as a function of liquid water velocity across the liquid−air interface, of $2J_0\xi^{1/2}$,[18] where $J_0 \simeq 1.3 \times 10^{-8}$ m$^{3/2}$/s is the evaporation rate.

As evaporation diverges near the contact line, a domain will always appear very near the contact line of typical extent ξ_c where the situation becomes critical (i.e., where the particle concentration $\bar{\Phi}$ equals the close-packing one: $\Phi_c = 60\%$, corresponding to $\phi_c \simeq 1350$ g/L). In this case, the viscosity at the contact line will become infinite, and the contact line can be pinned on this defect. Provided that our estimates of this typical size will remain smaller than the particle size d, we can assume that no stick−slip will occur. Inversely, if this typical size is larger than d, then stick−slip is to be expected.

To simplify the calculations of ξ_c, we now assume that the upstream concentration supplied by the recirculation at scales larger than ξ_c is close to the initial concentration $\Phi(\xi)) \simeq \Phi_0$, whereas at scales smaller than ξ_c the concentration observed at the contact line reads $\overline{\Phi(\xi)} \simeq \Phi_c$. The typical size of the defect ξ_c is then given by the balance of solvent fluxes:

$$(1 - \Phi_0)Q' = (1 - \Phi_c)Q + 2J_0\xi_c^{1/2} \quad (1)$$

Moreover, the particle concentration is stationary. The number of particles coming into the wedge is then exactly compensated for by the number coming out of the wedge, which reads

$$Q\Phi_c = Q'\Phi_0 \quad (2)$$

The combination of eqs 1 and 2 then gives a typical solid defect size ξ_c, which can be written as a function of the flow rate Q. In turn, Q can be related to the velocity U and local thickness $h \simeq \theta\xi$ by using standard lubrication theory inside a corner,[17] $Q \simeq 0.2Uh$. This finally gives an estimated defect size of

$$\xi_c \simeq \left(\frac{\Phi_0}{\Phi_c - \Phi_0}\frac{10J_0}{U\Theta}\right)^2 \quad (3)$$

The problem is now to introduce a criterion for the contact line whether it is pinned or not on the substrate by this defect. We can consider that a defect exists and is able to pin the contact line as soon as its size is larger than the diameter $d = 90$ nm of one particle. This gives a critical velocity U_c below which no pinning, and thus no stick−slip, will occur:

$$U_c \simeq \frac{10J_0}{\Theta d^{1/2}}\frac{\Phi_0}{\Phi_c - \Phi_0} \quad (4)$$

To be exact, the calculation should be performed following a slide of liquid at a concentration $\Phi(x)$ that increases in the vicinity of the contact line. The approach that we have chosen is more rough but allows us to understand the global mechanism. The critical velocity is plotted in Figure 3b as a solid line superimposed on the phase diagram. There is no adjustable parameter, so the order of magnitude is in very good agreement with our measurements despite the coarse-grained approach.

Let us here note that, to be exact, the calculation should be performed following a slide of liquid at a concentration $\Phi(x)$ that increases in the vicinity of the contact line. We have checked that this more complicated approach does not change the final result by more than 10%. The model proposed above is enough to capture the main physical mechanisms of the problem with a reasonable degree of complexity.

Finally, an interesting remark emerges from experiment: when the velocity is higher than U_c, the deposit cannot pin the contact line, and the drop is advancing just as if the liquid was pure

(16) Huh, C., Scriven, L. E. *J. Colloid Interface Sci.* **1971**, *35*, 85.
(17) de Gennes, P. G. *Z. Kolloid Polym. Sci.* **1984**, *264*, 463.
(18) $2J_0\xi^{1/2} = \int_0^\xi J_0 x^{-1/2}\,dx$
(19) The calculation of J_0 is a complicated problem. An estimation of this parameter can be obtained using diffusion-limited evaporation within laminar air flow. The evaporation rate thus reads $J(x) = J_0x^{-1/2}$ with $J_0 \propto \sqrt{D_g}\sqrt{U_{air}}c_v^{sat}/\rho_w$, where D_g is the diffusion coefficient of water in air, U_{air} is the velocity of the laminar air flow (estimated to be around 10 m/s here), c_v^{sat} is the saturation concentration of water in air, and ρ_w is the volume mass of water. The factor of proportionality is tabulated.[20] Such an approach gives $J_0 = 1.3 \times 10^{-8}$ m$^{3/2}$/s.
(20) Bird, R. B.; Stewart, W. E.; Lightfoot, E. N. *Transport Phenomena*; Wiley: New York, 1960.

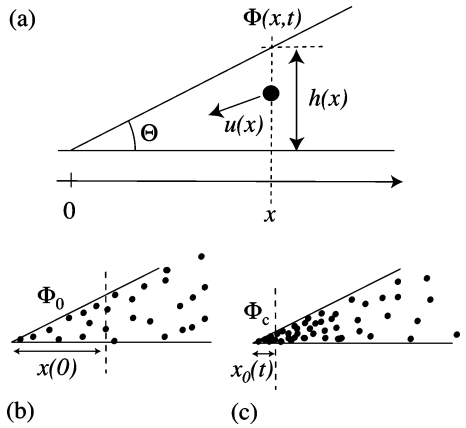

Figure 6. (a) Notation used to describe the trajectory of a particle inside the liquid wedge. (b) Initial concentration at time $t = 0$: the concentration is homogeneous. (c) Situation at time t: particles are concentrated at the contact line generating a solid defect of size x_0 if the concentration is greater than Φ_c. All of the particles inside the solid defect come from a distance smaller than $x(0)$ from the contact line.

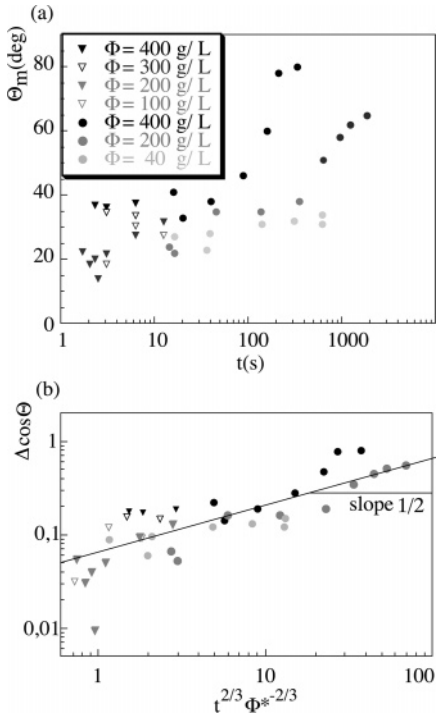

Figure 7. (a) Variation of Θ_m with the concentration and plate velocity. (b) Variation of the amplitude of the stick−slip ($\Delta(\cos\Theta)$) vs the expected power law depending on the time t and the normalized concentration Φ^*. The black line represents a power of $^1/_2$. It seems to describe the relationship between Θ and the quantity $t^{2/3}\Phi^{*-2/3}$ well. Note that to access a larger range of time t some of the measurements (circles) have been performed on inflated droplets, which allows us to control the pinning time very accurately.

water, with a contact angle very close to the one observed with a pure water drop (Figure 3). This means that the particle concentration influences neither the hydrodynamics nor the surface tension and that only the particle accumulation linked to evaporation affects the wetting dynamics.

3.2. Stick-Slip Regime. The former calculation allows us to exhibit a frontier between the pinning and sliping cases. A crucial problem is now to describe the regular stick−slip motion of the contact line at low velocity and high concentration. The following calculation therefore allows us to estimate the amplitude of stick−slip in terms of the contact angle oscillation amplitude.

We now consider a contact line, in the stick−slip regime, just after a jump between its two extreme positions. Let us first write the size of the deposit depending of the contact line pinning time. The evaporation flux $J(x) = J_0 x^{-1/2}$ drives the particles toward the contact line by advection. We consider in all of the calculation that the contact angle is constant, which is an approximation but gives the same scaling for the deposit size.

Let us consider a particle at a distance $x(t)$ from the contact line. Advection drives this particle at a speed $U = -\mathrm{d}x/\mathrm{d}t = J_0 x^{-1/2}$. The integration of this equation gives the particle trajectory

$$x(t) = \left(-\frac{3}{2}J_0 t + x(0)^{3/2}\right)^{2/3} \tag{5}$$

where $x(0)$ is the particle position at $t = 0$. The particle concentration at the contact line accounts for a solid defect as soon as the mean concentration is greater than Φ_c. The size $x_0(t)$ of this solid defect grows with the time. To calculate $x_0(t)$, let us consider Figure 6b and c: at a time t, all of the particles forming the defect come from a distance smaller than $x(0)$ from the contact line. Simple mass conservation gives the following equation:

$$\Phi\Theta x(0)^2 = \Phi_c \Theta x_0(t)^2 \tag{6}$$

The size of the defect can be deduced from eqs 5 and 6 (if $x_0(t)$ is identified with respect to $x(t)$):

$$x_0(t) = \left(\frac{\frac{3J_0}{2}}{\left(\frac{\Phi_c}{\Phi_0}\right)^{3/4} - 1}\right)^{2/3} t^{2/3} \tag{7}$$

In the following discussion, we will focus only on the scaling law

$$x_0(t)^{3/2} \propto \frac{t}{\Phi^*} \tag{8}$$

where

$$\Phi^* = \left(\frac{\Phi_c}{\Phi_0}\right)^{3/4} - 1$$

This law then gives the scaling of the deposit size that we want to relate to the stick−slip amplitude. The latter is the variation of Θ during a period of stick−slip (i.e., $\Delta\Theta = \Theta_m - \Theta_e$, where $\Theta_e \simeq 10°$ is the equilibrium contact angle and Θ_m is the maximum contact angle that is observed when the contact line is depinned; see Figure 2).

In an oversimplified view, which is helpful here, Θ_e is given by the well-known Young relation: $\cos\Theta_e = (\gamma_{sg} - \gamma_{sl})/\gamma$ where γ_{sg}, γ_{sl}, and γ are the solid/gas, solid/liquid, and liquid/gas surface tensions, respectively. From this point of view, the variation of the contact angle from Θ_e to Θ_m is due to a force f modifying this equilibrium. In turn, f is due to the force $f_{pinning}$ exerted by the deposition on the contact line.

Because of our lack of knowledge of the defect structure, we have no simple law available to link theoretically the size of the deposit to the force f, but we can invert the problem and deduce this law from experiment.

The maximum variation of $\Delta(\cos\Theta)$, which can be measured through the stick−slip amplitude, is plotted in Figure 7 as a function of the wrinkle size, predicted by eq 8. Note that we performed experiments on pushed droplets that exhibit regular stick−slip (triangles) but also on inflated droplets (circles) to

reach larger values of time t. Concerning pushed droplets, the plotted time is built on the drop velocity: $t = {}^{L}/_{U}$ where $L = 6$ mm is the typical droplet size. A scaling law can be extracted from the plot:

$$\Delta(\cos\Theta) \propto \sqrt{t^{2/3}\Phi^{*-2/3}} \quad (9)$$

This scaling, which seems to lead to a good collapse of the data in Figure 7, implies that the force f_{pinning} exerted by the defect on the contact line scales as $\sqrt{(x_0)}$. This is a nontrivial result that would now need to be interpreted in terms of the defect structure, which remains outside of the scope of the present article.

To summarize, though we cannot completely solve the problem, the comparison between our model and the experiment has allowed us to relate the contact angle variation with time across the scaling law[9] and to get information on the force exerted by the defect on the contact line.

Note that in eq 9 $\Delta(\cos\Theta)$ is a dimensionless quantity, proportional to x_0, so a regularizing length l has to be introduced such that $\Delta(\cos\Theta) = x_0/l$. The value of $\Delta(\cos\Theta)$ corresponding to $t^{2/3}\Phi^{*-2/3} \simeq 10$ is 0.1 (Figure 7), and l is then found to be around 1 mm, which is a third of the capillary length. This length is also possibly linked to the size of the drop in a way that remains to be understood.

Finally, eq 8 allows us to calculate the order of magnitude of the expected size of the defect. Let us take a typical value of the quantity $t^{2/3}\Phi^{*-2/3}$ of around 10 from Figure 7. We can then calculate a typical size x_0 of the defect to be around 100 μm. Note that in Figure 4 the observed colloidal wrinkle is exactly this size. The value of $\Delta(\cos\Theta)$ corresponding to $t^{2/3}\Phi^{*-2/3} \simeq 10$ is 0.1 (Figure 7).

4. Conclusions

This article presents the first experiments, to our knowledge, combining an advancing contact line with a colloidal suspension. These have been performed on pushed droplets. We have exhibited a competition between drying and hydrodynamic flow. Drying accounts for contact line pinning through particle agglomeration whereas hydrodynamic flow renews the solution while the contact line advances. The competition between both phenomena leads to two regimes. At high velocity and low colloid concentration, the contact line advances continuously with a contact angle very close to the one observed on a drop of pure water. At low velocity or large concentration, the contact line is pinned from time to time, and a stick−slip motion appears. The comparison of both terms gives a critical speed U_c that splits both regimes. The calculated critical speed is of the same order of magnitude as the one observed experimentally.

SEM visualizations of the particle deposition have shown that this stick−slip motion accounts for particle wrinkles corresponding to each period. Another calculation has allowed us to calculate the size x_0 of this wrinkle as a function of time as soon as the contact line is pinned. The comparison of the obtained prediction to our data predicts that the pinning force exerted by the wrinkle on the contact line is proportional to $\sqrt{x_0}$. The verification of this hypothesis is beyond the scope of the present article and would necessitate more systematic SEM imaging of the colloidal wrinkle formed at the contact line.

Acknowledgment. We thank St. Gobain-Recherche for financial support as well as M.-I. Watchi for having performed the S.E.M. experiments and for stimulating discussions. We also thank D. Vallet, D. Pradal, O. Brouard and J.-C. Guibert for help in the conception and perfomance of the experiment. We are finally grateful to Guillaume Berteloot, who performed complementary experiments providing evidence of the importance of evaporation in our system.

LA052989E